Strain in van der Waals epitaxy and evidence for a collective macroscopic effect of a negligibly small perturbation

Zhili Zhu, Ping Cui, Yu Jia, Shengbai Zhang, and Zhenyu Zhang

Phys. Rev. B **100**, 035429 — Published 22 July 2019

DOI: 10.1103/PhysRevB.100.035429

Strain in van der Waals epitaxy and evidence of collective macroscopic effect of a negligibly small perturbation

Zhili Zhu[1,2], Ping Cui[2], Yu Jia[1], Shengbai Zhang[2,3*], and Zhenyu Zhang[2*]
[1] *International Laboratory for Quantum Functional Materials of Henan, and School of Physics and Engineering, Zhengzhou University, Zhengzhou 450001, China*
[2] *ICQD, Hefei National Laboratory for Physical Sciences at the Microscale, and Synergetic Innovation Center of Quantum Information and Quantum Physics, University of Science and Technology of China, Hefei, Anhui 230026, China*
[3] *Department of Physics, Applied Physics, & Astronomy, Rensselaer Polytechnic Institute, Troy, New York 12180, USA*

(Dated: July 9, 2019)

Recent studies of van der Waals heterostructures involving transition metal dichalcogenide (TMD) overlayers have revealed the formation of highly ordered mirror twin boundaries (MTBs) dividing domains in single 2H phase. Here, using a multi-scale modeling approach we identify that the MTB network formation results from a delicate interplay between strain accumulation in the heterostructure and single crystal preference of the growing overlayer. We determine the energy costs for the creation of the MTB by first-principles calculations, from which we show that even the presence of a perceived-to-be negligible strain is able to induce the formation of the MTB networks as an effective strain relief mechanism of the growing TMD monolayers, as observed experimentally. This counterintuitive finding demonstrates the importance of collective effects in weakly-interacting systems, i.e., in van der Waals epitaxy.

PACS numbers: 68.55.-a, 68.35.Rh, 61.46.-w,

I. INTRODUCTION

Since the discovery of graphene via mechanical exfoliation [1], fabrication of a rapidly increasing number of new types of two-dimensional (2D) materials [2–6] and their heterostructures [7] has been the subject of intensive research. In this endeavor, much effort has been devoted to the growth of the layered materials on proper substrates, including catalytically more active substrates such as a copper foil [8, 9] and relatively inert surfaces such as graphite [10]. In either case, the coupling between the growing 2D monolayer (ML) and the substrate is rather weak, characterizing the process as van der Waals (vdW) epitaxy [11]. As a relatively new category of non-equilibrium growth phenomena, the versatility of vdW epitaxy remains to be fully exploited in fabricating various 2D materials and heterostructures with diverse properties and functionalities [12–16].

Among the different materials compositions, the vdW growth of transition metal dichalcogenides (TMDs) is particularly appealing, largely because such systems exhibit emergent exotic properties in the 2D regime or in heterostructural geometry [17–20]. Here, one striking observation was the self-organized growth of highly ordered mirror twin boundaries (MTBs) in vdW epitaxy of TMD MLs on graphite [10] or different TMDs [21, 22] or substrates. Subsequent studies have revealed intriguing properties of such MTBs, including their metallicity and charge density waves (CDW) behavior [23], which can be further exploited for potential applications such as enhanced catalysis. Yet to date, the underlying formation mechanism(s) of such MTB networks remains to be identified. Past effort has been focused on the creation of chalcogen vacancies and their evolutions during the growth [24–26], while the potential role of strain has been neglected, mainly because the vdW interfacial coupling in such systems is much weaker than the typical chemical bonding strengths in traditional epitaxy.

In this paper, we use a multi-scale modeling approach to demonstrate that the underlying formation mechanism of the MTB networks lies in a delicate but physically important interplay between the strain accumulation in the heterostructure and single crystal preference of the overlayer. We first use first-principles calculations to systematically investigate the formation energies of the MTBs in different TMD MLs. Next, we show that, in contradiction to the widely-held belief, even a moderate strength of strain in the heterostructures is sufficient to induce the formation of the MTB networks as an effective strain relief mechanism of the growing TMD MLs, consistent with the experimental observations. We further determine the periodicity of the MTB networks quantitatively, and predict the formation of MTBs in a given TMD ML upon proper strain engineering.

The paper is organized as follows. In Sec. II, we describe the first-principles methods and the structural model of the MTB networks. In Sec. III, We calculate the formation energy of the MTB networks and strain energy in the TMD monolayers using density functional theory (DFT). Using these DFT results as inputs, combining with the continuum elasticity theory, we demonstrate that the presence of even a moderate

stress is sufficient to induce the formation of the MTBs as an effective strain relief mechanism in TMD overlayers. The validity of the mechanism is further confirmed by close comparisons with experimental observations. In Sec. IV, we conclude this work with a brief summary.

II. COMPUTATIONAL DETAILS

The density functional theory (DFT) calculations were carried out using the Vienna *ab initio* simulation package (VASP). For the ion-electron interaction, we used the projector augmented wave method [27, 28], while for the exchange-correlation energy, we used the Perdew-Burke-Ernzerhof functional [29]. The kinetic-energy cutoff for the plane wave basis set was chosen to be 400 eV. At a higher cutoff energy of 500 eV, the calculated strain properties are unchanged with respect to those of 400 eV. The ordered MTB networks were modeled using periodic slab geometries with 20 Å thick vacuum layers to separate adjacent TMDs. The lattice constants and atom positions were fully relaxed until the Hellmann-Feynman forces were less than 0.01 eV/Å.

III. RESULTS AND DISCUSSION

To identify the likely formation mechanism of the MTB network, we first obtain its formation energy in a TMD ML, taking $MoSe_2$ as a prototypical system. It has been observed experimentally that, during epitaxial growth of $MoSe_2$ on HOPG, periodic networks were formed, composed of domains in the 2H phase divided by MTB lines [10]. As shown in Fig. 1(a), we construct an atomistic model with periodic MTB lines embedded in a $MoSe_2$ ML to simulate the experimentally observed patterns. Within a 1D MTB line, the smallest unit is highlighted in Fig. 1(b). The stoichiometric ratio of Mo:Se in the MTB lines is 1:1, indicating an Se deficiency from the ideal $MoSe_2$ structure. The formation energy of the MTB network with respect to the 2H phase $MoSe_2$ can be defined as

$$E_{\rm f} = E_{\rm tot} + 2N\mu_{\rm Se} - N_{\rm Mo}E_{\rm MoSe_2} \qquad (1)$$

where $E_{\rm tot}$ is the total energy of the supercell, N is the number of the MTB units within each MTB line (i.e., the supercell size), $\mu_{\rm Se}$ is the chemical potential of Se, $N_{\rm Mo}$ is the number of Mo atoms in the supercell, and $E_{\rm MoSe_2}$ is the energy of pristine $MoSe_2$ per formula unit. Here, $\mu_{\rm Se}$ is determined by $\mu_{\rm Mo} + 2\mu_{\rm Se} = E_{\rm MoSe_2}$, whose range is limited by the Se_8 molecule and the Mo bulk phase, corresponding to the Se-rich end and Se-poor limit, respectively. While evidently chalcogen chemical potential is an important parameter, as evidenced by the calculated formation energy of the MTB unit shown in Fig.2. It is worth noting that, although the flux ratio of X:M (X=S, Se, Te; M=Mo, W) is usually tens to hundreds during epitaxial growth of TMDs, a low residence time of the X atoms on the surface before re-evaporation may result in the deficiency of the X atoms [21]. Without loss of generality, here we adopt the value of $\mu_{\rm Se}$ at the Se-poor limit in the following calculations.

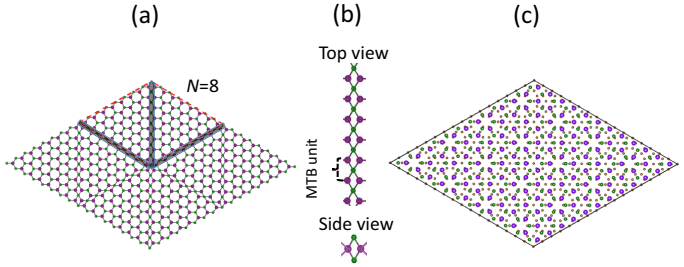

FIG. 1: (a) A schematic model of the MTB network in a $MoSe_2$ monolayer, with the supercell highlighted by the red dashed frame, and three equivalent MTB segments by gray stripes, respectively; the lateral supercell size is N=8 for illustration. (b) Top and side views of the atomic structure of an MTB line, with the MTB unit indicated. (c) Schematic of the moiré pattern formation due to the atomic lattice mismatch between the $MoSe_2$ overlayer and graphene substrate.

The calculated formation energy of the MTB network in a $MoSe_2$ ML as a function of the supercell size N is shown in Fig. 2(a), which can be fitted as $E_{\rm f} = aN + b$, with a = 0.56 eV and b = 1.96 eV. The formation energy of the MTB unit ($E_{\rm MTB}$) can then be obtained from the slope, given by $E_{\rm MTB}$ = a/3 = 0.19 eV, since each supercell contains three equivalent MTB segments which are highlighted by gray stripes in Fig. 1(a). Furthermore, we can interpret the intersection of the linear plot to be the corner energy [30] of the MTB, given by $E_{\rm corner}$ = b = 1.96 eV. We therefore can rewrite the formation energy of the MTB network as

$$E_{\rm f} = 3NE_{\rm MTB} + E_{\rm corner} \qquad (2)$$

Similar to $MoSe_2$, MTB networks have also been observed in epitaxial growth of $MoTe_2$ MLs on MoS_2 [21]. Using the same procedure, we obtain the formation energy ($E_{\rm f}$) of the MTB networks in $MoTe_2$ as a function of N as shown in Fig. 2(a), which can again be fitted with a linear relationship. The corresponding energy per MTB unit and corner energy are given by $E_{\rm MTB}$ = -0.01 eV and $E_{\rm corner}$ = 0.65 eV, respectively. Here we note that $E_{\rm f}$, $E_{\rm MTB}$, and $E_{\rm corner}$ are all much lower than those in the $MoSe_2$ case, and $E_{\rm MTB}$ is even negative at the Te-poor limit, both observations indicating the relative easiness for the formation of the MTB networks in $MoTe_2$. We have also calculated the formation energies of the MTB networks in MoS_2, WS_2, and WSe_2 MLs, all of which possess the 2H phase as the stable structure. The results are shown in Fig. 2, exhibiting the distinct contrast that the formation energies are much higher in these latter three systems.

To gain a deeper understanding of the formation energies of such MTBs, we obtain $E_{\rm MTB}$ for different 2D MX_2 (M=Mo, W, X=S, Se, Te) MLs, as listed in Table I. Several interesting observations can be made. First, $E_{\rm MTB}$ exhibits the trend $E_{\rm MTB}(MS_2) > E_{\rm MTB}(MSe_2) > E_{\rm MTB}(MTe_2)$ for both the Mo

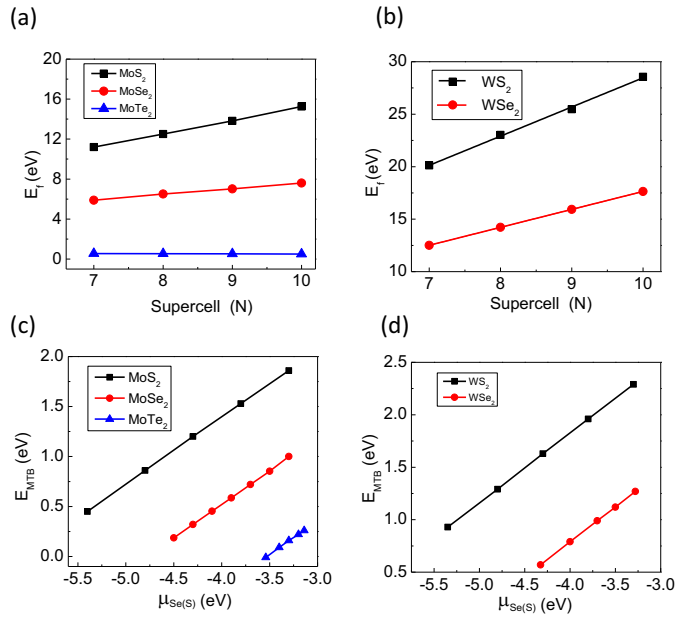

FIG. 2: (a) Formation energy (E_f) of the MTB network in MoS_2, $MoSe_2$, or $MoTe_2$ MLs as a function of the supercell size N at the chalcogen poor limit. (b) Similar to (a), but for WS_2 and WSe_2. (c) Formation energy of the MTB unit in MoS_2, $MoSe_2$, or $MoTe_2$ MLs as a function of chalcogen chemical potential. (d) Similar to (c), but for WS_2 and WSe_2.

and W series. Second, for a given X, we have $E_{\mathrm{MTB}}(WX_2) > E_{\mathrm{MTB}}(MoX_2)$. Third, $MoSe_2$ and $MoTe_2$ exhibit the lowest formation energies per MTB unit, which at least partially explain why MTB networks have been observed in these systems. Fourth, E_{MTB} is much higher for MoS_2, W_2, and WSe_2, which may explain why no such MTB network has been reported in these systems. Finally, the corner energy also varies significantly from system to system, and its effect may not be neglected, as in the case of $MoTe_2$ where the corner energy even dominates.

TABLE I: Lattice constant (d), energy per MTB unit (E_{MTB}), corner energy (E_{corner}), and in-plane Youngs modulus ($C_{2\mathrm{D}}$) for different TMD MLs.

System	d (Å)	E_{MTB} (eV)	E_{corner} (eV)	$C_{2\mathrm{D}}$ (eV/Å^2)
MoS_2	3.18	0.44	1.73	20.9
$MoSe_2$	3.32	0.19	1.96	18.4
$MoTe_2$	3.55	-0.11	0.65	12.5
WS_2	3.18	0.93	0.67	22.4
WSe_2	3.32	0.57	0.61	19.3

Next, we return to the potential formation mechanism of such MTB networks in the TMD heterostructures. In a traditional heteroepitaxy involving strong interfacial chemical bonding, it has been well recognized that a strain relief can serve as the dominant driving force in inducing the formation of highly ordered patterns such as the dislocation networks in a growing overlayer on a lattice-mismatched substrate [31]. In contrast, for the formation of such the MTB networks in TMDs MLs, the potential role of the strain has been neglected due to the apparent weak vdW nature of the interfacial couplings [22, 32]. However, more recent studies have provided overwhelming evidence that the strain accumulated at the interfaces of different vdW heterostructures can greatly influence their electronic, optical, and other properties [17–20, 33–35]. Here we demonstrate that such strain accumulations can also serve as the dominant driving force in the morphological evolution of the growing TMD MLs in vdW epitaxy, as manifested by the formation of the MTB networks, as given below.

We assess the strain effects using a multi-scale modeling approach. First, we use first-principles calculations to obtain the strain energy variations of different TMD MLs upon compressive or tensile strain. The results are shown in Fig. 3, exhibiting dominant harmonic behavior for strain within $\pm 2\%$.

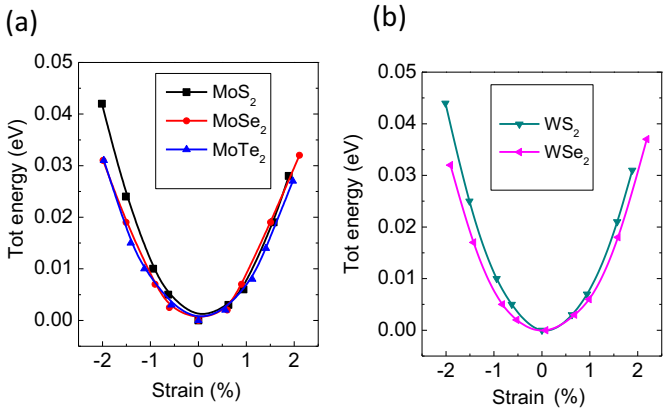

FIG. 3: (a) Strain energy per formula unit as a function of the strain for different MoX_2 MLs (X=S, Se, Te). (b) Similar to (a), but for WS_2 and WSe_2.

Next, using the DFT results, we extend the study to the regime of continuum elasticity theory by obtaining the in-plane Youngs modulus ($C_{2\mathrm{D}}$) for each system as [36].

$$C_{2\mathrm{D}} = \frac{1}{A_0}\left(\frac{\partial^2 E_s}{\partial \varepsilon^2}\right) \tag{3}$$

where E_s, A_0, and ε are strain energy, area of the unit cell, and strain, respectively. The results are given in Table I, showing that the Youngs moduli of four of the systems are comparable to each other, with that of $MoTe_2$ to be substantially softer. The strain energy per unit cell is obtained by an integration of Eq. (3). Under the harmonic approximation, both integration constants are zero, so $E_s = \frac{1}{2}A_0 C_{2D}\varepsilon^2$. The total strain energy is thus

$$E_s^N = \frac{1}{2}A_0 C_{2D}\varepsilon^2 N^2 \tag{4}$$

where N is the lateral size of the supercell. The same equation has been derived and applied to the study of carbon nanotubes [37].

The underlying formation mechanism of the MTB networks can now be understood from the competition between the strain energy accumulation and single crystal preference of the TMD MLs. As a strained ML grows, strain energy accumulates in the ML following Eq. (4). When its lateral size is too large, the system chooses to release the strain energy through the creation of MTBs, whose energy cost follows Eq. (2). The energy balance $E_s = E_f$ between the two determines the critical size as shown in Fig. 4, above which the formation of the MTB network is energetically favored.

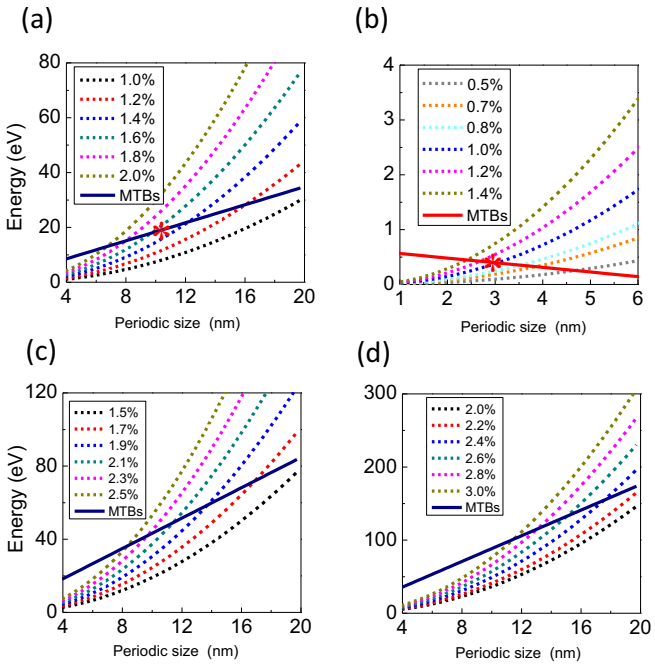

FIG. 4: Strain energy (E_s) at different strains (dashed curves) and formation energy of the MTB networks (E_f) (solid line) as a function of the lateral size of a growing ML for (a) $MoSe_2$, (b) $MoTe_2$, (c) MoS_2, and (d) WS_2. The red stars in (a) and (b) indicate the experimentally observed periods of the MTB networks, from which the corresponding strain can be estimated.

To further illustrate the physical validity of the strain relief mechanism, we take the experimental observations as a crosscheck, as applied to the MTB networks formed in $MoSe_2$ and $MoTe_2$ MLs. As shown in Fig. 4(a), the experimentally observed size ($\sim$ 10 nm) of the MTB network in a $MoSe_2$ ML [10] corresponds to the strain of $\sim$ 1.5% (red star). As shown in Fig. 1(c), the most probable superlattice at the interface is a 3×3 $MoSe_2$ superstructure on a 4×4 HOPG superstructure, with a misfit strain of $\sim$ 0.5%, forming a moiré pattern with the period of $\sim$ 10 Å. Therefore, additional strain corresponding to the stress of $\sim$ 1% should have been built into the growing overlayer during non-equilibrium growth, which is physically highly feasible. Furthermore, as shown in Fig. 4 (b), only a moderate strain of $\sim$ 1% is sufficient to induce the formation of the MTB network in a growing $MoTe_2$ ML with the experimentally observed period of $\sim$ 2.8 nm [21].

Based on the formation mechanism established above, some remarkable tunabilities on the formation of the MTB networks may be achieved. For systems that support the formation of MTB networks, one can effectively tune the network sizes by changing the strain to modify the periods of the networks for more desirable functionalities. Such strain variations can be obtained by proper choices of the substrates, or by changing the growth conditions, or by applying external stress, or, by a combination of the different approaches. In this regard, the emergence of external-stress-induced MTB networks in a growing TMD ML of a vdW heterostructure that otherwise does not support MTB formation will serve as a compelling validation of the mechanism emphasized here. In particular, based on Figs. 4(d), we expect that the formation of the MTB networks in a WS_2 ML will be highly unlikely in the typical vdW heterostructures, because it requires a too high stress (e.g., well over 2%) but proper applications of an external stress will likely make it happen.

IV. CONCLUSION

In summary, we have identified the MTB network formation mechanism to be originated from a delicate balance between strain accumulation in the heterostructure and single crystal preference of the overlayer. The key is to employ a multiscale approach where the formation energy of the MTB networks in different TMD monolayers and the strain energy variations in growing TMD monolayers are evaluated by DFT calculations from which, the continuum elasticity theory analyses can be applied to demonstrate that even a moderate strain is enough to induce the formation of the MTBs observed by experiments. The breakthrough in understanding the unconventional role of strains in vdW epitaxy opens the door for tuning the MTB networks for unprecedented control of the physical properties of TMDs and other 2D materials via strain engineering.

Work in China was mainly supported by the NSFC (Grant Nos. 11634011, 11722435, 61434002, and 11774078), the NSF of Henan Province of China (Grant No.162300410254), the National Key Basic Research Program of China (Grant No. 2017YF0303500), and the Strategic Priority Research Program of Chinese Academy of Sciences (Grant No. XDB30000000). S.B.Z. was supported by the US NSF (Grant No. DMREF-1627028).

* Corresponding authors: zhangs9@rpi.edu, zhangzy@ustc.edu.cn.

[1] K. S. Novoselov, A. K. Geim, S. V. Morozov, D. Jiang, Y. Zhang, S. V. Dubonos, I. V. Grigorieva, and A. A. Firsov, Science **306**, 666 (2004).

[2] P. Vogt, P. De Padova, C. Quaresima, J. Avila, E. Frantzeskakis, M. C. Asensio, A. Resta, B. Ealet, and G. Le Lay, Phys. Rev. Lett. **108**, 155501 (2012).

[3] L. Li, Y. Yu, G. J. Ye, Q. Ge, X. Ou, H. Wu, D. Feng, X. H. Chen, and Y. Zhang, Nat. Nanotechnol. **9**, 372 (2014).

[4] A. J. Mannix, X. F. Zhou, B. Kiraly, J. D. Wood, D. Alducin, B. D. Myers, X. Liu, B. L. Fisher, U. Santiago, and J. R. Guest, Science **350**, 1513 (2015).

[5] F.-f. Zhu, W.-j. Chen, Y. Xu, C.-l. Gao, D.-d. Guan, C.-h. Liu, D. Qian, S.-C. Zhang, and J.-f. Jia, Nat. Mater. **14**, 1020 (2015).

[6] Z. L. Zhu, X. Cai, S. Yi, J. Chen, Y. Dai, C. Niu, Z. Guo, M. Xie, F. Liu, J. H. Cho, Y. Jia, and Z. Y. Zhang, Phys. Rev. Lett. **119**, 106101 (2017).

[7] A. K. Geim and I. V. Grigorieva, Nature **499**, 419 (2013).

[8] X. Li, W. Cai, J. An, S. Kim, J. Nah, D. Yang, R. Piner, A. Velamakanni, I. Jung, and E. Tutuc, Science **324**, 1312 (2009).

[9] H. Chen, W. Zhu, and Z. Y. Zhang, Phys. Rev. Lett. **104**, 186101 (2010).

[10] H. Liu, L. Jiao, F. Yang, Y. Cai, X. Wu, W. Ho, C. Gao, J. Jia, N. Wang, and H. Fan, Phys. Rev. Lett. **113**, 066105 (2014).

[11] A. Koma, Thin Solid Films **216**, 72 (1992).

[12] M. Li, Y. Shi, C. Cheng, L.Lu, Y. Lin, H. Tang, M. Tsai, C. Chu, K. Wei, J. He, W. Chang, K. Suenaga, L. Li, Science **349**, 524 (2015).

[13] K. S. Novoselov, A. Mishchenko, A. Carvalho, and A. H. Castro Neto, Science **353**, 9439 (2016).

[14] X. Lin, J. C. Lu, Y. Shao, Y. Y. Zhang, X. Wu, J. B. Pan, L. Gao, S. Y. Zhu, K. Qian, Y. F. Zhang, D. L. Bao, L. F. Li, Y. Q. Wang, Z. L. Liu, J. T. Sun, T. Lei, C. Liu, J. O. Wang, K. Ibrahim, D. N. Leonard, W. Zhou, H. M. Guo, Y. L. Wang, S. X. Du, S. T. Pantelides, and H. J. Gao, Nat. Mater. **16**, 717 (2017).

[15] Y. Liu, J. Guo, E. Zhu, L. Liao, S.-J. Lee, M. Ding, I. Shakir, V. Gambin, Y. Huang, and X. Duan, Nature **557**, 696 (2018).

[16] Y. Liu, Y. Huang, and X. Duan, Nature **567**, 323 (2019).

[17] K. Tran, G. Moody, F. Wu, X. Lu, J. Choi, K. Kim, A. Rai, D. A. Sanchez, J. Quan, A. Singh, J. Embley, A. Zepeda, M. Campbell, T. Autry, T. Taniguchi, K. Watanabe, N. Lu, S. K. Banerjee, K. L. Silverman, S. Kim, E. Tutuc, L. Yang, A. H. MacDonald, and X. Li, Nature **567**, 71 (2019).

[18] C. Jin, E. C. Regan, A. Yan, M. Iqbal Bakti Utama, D. Wang, S. Zhao, Y. Qin, S. Yang, Z. Zheng, S. Shi, K. Watanabe, T. Taniguchi, S. Tongay, A. Zettl, and F. Wang, Nature **567**, 76 (2019).

[19] K. L. Seyler, P. Rivera, H. Yu, N. P. Wilson, E. L. Ray, D. G. Mandrus, J. Yan, W. Yao, and X. Xu, Nature **567**, 66 (2019).

[20] L. Britnell, R. M. Ribeiro, A. Eckmann, R. Jalil, B. D. Belle, A. Mishchenko, Y. J. Kim, R. V. Gorbachev, T. Georgiou, S. V. Morozov, A. N. Grigorenko, A. K. Geim, C. Casiraghi, A. H. C. Neto, and K. S. Novoselov, Science **340**, 1311 (2013).

[21] H. C. Diaz, Y. Ma, R. Chaghi, and M. Batzill, Appl. Phys. Lett. **108**, 1102 (2016).

[22] Y. Ma, S. Kolekar, H. Coy Diaz, J. Aprojanz, I. Miccoli, C. Tegenkamp, and M. Batzill, ACS Nano **11**, 5130 (2017).

[23] S. Barja, S. Wickenburg, Z.-F. Liu, Y. Zhang, H. Ryu, Miguel M. Ugeda, Z. Hussain, Z.-X. Shen, S.-K. Mo, E. Wong, Miquel B. Salmeron, F. Wang, M. F. Crommie, D. F. Ogletree, Jeffrey B. Neaton, and A. Weber-Bargioni, Nat. Phys. **12**, 751 (2016).

[24] J. Lin, S. T. Pantelides, and W. Zhou, ACS Nano **9**, 5189 (2015).

[25] O. Lehtinen, H. P. Komsa, A. Pulkin, M. B. Whitwick, M. W. Chen, T. Lehnert, M. J. Mohn, O. V. Yazyev, A. Kis, and U. Kaiser, ACS Nano **9**, 3274 (2015).

[26] S. Wang, G. D. Lee, S. Lee, E. Yoon, and J. H. Warner, ACS Nano **10**, 5419 (2016).

[27] G. Kresse and J. Hafner, Phy. Rev. B **48**, 13115 (1993).

[28] G. Kresse and J. Furthmller, Comp. Mater. Sci. **6**, 15 (1996).

[29] J. P. Perdew, K. Burke, and M. Ernzerhof, Phys. Rev. Lett. **77**, 3865 (1996).

[30] B. S. Swartzentruber, Y.-W. Mo, R. Kariotis, M. G. Lagally, and M. B. Webb, Phys. Rev. Lett. **65**, 1913 (1990).

[31] H. Brune, M. Giovannini, K. Bromann, and K. Kern, Nature **394**, 451 (1998).

[32] L. Jiao, H. J. Liu, J. L. Chen, Y. Yi, W. G. Chen, Y. Cai, J. N. Wang, X. Q. Dai, N. Wang, and W. K. Ho, New J. Phys. **17**, 53023 (2015).

[33] C. Zhang, C.-P. Chuu, X. Ren, M.-Y. Li, L.-J. Li, C. Jin, M.-Y. Chou, and C.-K. Shih, Sci. Adv. **3**, 1601459 (2017).

[34] C. Zhang, M.-Y. Li, J. Tersoff, Y. Han, Y. Su, L.-J. Li, D. A. Muller, and C.-K. Shih, Nat. Nanotechnol. **13**, 152 (2018).

[35] X. Li, M.-W. Lin, J. Lin, B. Huang, A. A. Puretzky, C. Ma, K. Wang, W. Zhou, S. T. Pantelides, M. Chi, I. Kravchenko, J. Fowlkes, C. M. Rouleau, D. B. Geohegan, and K. Xiao, Sci. Adv. **2**, 1501882 (2016).

[36] M. Topsakal, S. Cahangirov, and S. Ciraci, Appl. Phys. Lett. **96**, 091912 (2010).

[37] X. Zhou, J. Zhou, and Z. Ouyang, Phy. Rev. B **62**, 13692 (2000).